PNAS RESEARCH ARTICLE | GENETICS

Paf1 complex subunit Rtf1 stimulates H2B ubiquitylation by interacting with the highly conserved N-terminal helix of Rad6

Tasniem Fetian[a,1], Brendan M. McShane[a,1,2,3], Nicole L. Horan[a], Donya N. Shodja[a,4], Jason D. True[b,5], Amber L. Mosley[b], and Karen M. Arndt[a,6]

Edited by Jasper Rine, University of California Berkeley, CA; received November 23, 2022; accepted April 5, 2023

Histone modifications coupled to transcription elongation play important roles in regulating the accuracy and efficiency of gene expression. The monoubiquitylation of a conserved lysine in H2B (K123 in *Saccharomyces cerevisiae*; K120 in humans) occurs cotranscriptionally and is required for initiating a histone modification cascade on active genes. H2BK123 ubiquitylation (H2BK123ub) requires the RNA polymerase II (RNAPII)-associated Paf1 transcription elongation complex (Paf1C). Through its histone modification domain (HMD), the Rtf1 subunit of Paf1C directly interacts with the ubiquitin conjugase Rad6, leading to the stimulation of H2BK123ub in vivo and in vitro. To understand the molecular mechanisms that target Rad6 to its histone substrate, we identified the site of interaction for the HMD on Rad6. Using in vitro cross-linking followed by mass spectrometry, we localized the primary contact surface for the HMD to the highly conserved N-terminal helix of Rad6. Using a combination of genetic, biochemical, and in vivo protein cross-linking experiments, we characterized separation-of-function mutations in *S. cerevisiae RAD6* that greatly impair the Rad6–HMD interaction and H2BK123 ubiquitylation but not other Rad6 functions. By employing RNA-sequencing as a sensitive approach for comparing mutant phenotypes, we show that mutating either side of the proposed Rad6–HMD interface yields strikingly similar transcriptome profiles that extensively overlap with those of a mutant that lacks the site of ubiquitylation in H2B. Our results fit a model in which a specific interface between a transcription elongation factor and a ubiquitin conjugase guides substrate selection toward a highly conserved chromatin target during active gene expression.

Paf1 complex | Rad6 | Rtf1 | histone H2B ubiquitylation | transcription

Histone posttranslational modifications (PTMs) are key to chromatin regulation during gene expression. The attachment of chemical groups or peptides to specific histone residues controls recruitment of regulatory proteins to nucleosomes and imposes structural changes to chromatin (1). The deposition of histone PTMs, like ubiquitylation, methylation, acetylation, and phosphorylation, typically involves a network of participating proteins. A prominent example is the monoubiquitylation of histone H2B on K123 in *Saccharomyces cerevisiae* or K120 in mammals. The reversible ubiquitylation of H2B occurs cotranscriptionally and its level reflects the elongation rate of RNA polymerase II (RNAPII) (2–4). H2BK123ub is important for nucleosome stability during transcription elongation in vivo, likely in coordination with the histone chaperone FACT, and poses an energetic barrier to RNAPII in vitro (5–8). Through a cross talk mechanism, H2BK123ub is required for the di- and tri-methylation of H3K4 and H3K79 via the Set1 and Dot1 methyltransferases, respectively (9–13). In turn, H3K4me2 and H3K4me3 recruit histone acetyltransferase and deacetylase complexes, further modulating chromatin accessibility (14–16).

The ubiquitin conjugase (E2) Rad6, the ubiquitin ligase (E3) Bre1, and the Bre1associated protein Lge1 are required for H2BK123ub in *S. cerevisiae*, and homologs of Rad6 and Bre1 function analogously in other eukaryotes, including humans (17–21). As an E2, Rad6 coordinates with different E3 proteins to ubiquitylate substrates within diverse biochemical pathways. This is reflected in the numerous mutant phenotypes associated with *rad6* mutants. For example, in yeast, null alleles of *rad6* affect silencing of transcription near telomeres (18, 22), postreplication repair of DNA damage (23), protein degradation dependent on the N-degron pathway (24, 25), response to oxidative stress (26, 27), and Ty1 element transposition (28, 29).

During transcription elongation, RNAPII interacts with regulatory proteins that cotranscriptionally modulate its activity and/or the local chromatin environment. The evolutionarily conserved, multifunctional Paf1C, comprised of five subunits in yeast (Paf1, Rtf1, Ctr9, Cdc73, and Leo1), is a core component of the RNAPII active elongation complex that facilitates transcription elongation across eukaryotic genomes (30). In

Significance

Transcription by RNAPII is tightly coordinated with mechanisms that control chromatin structure. Disruption of this interplay leads to deleterious effects on gene expression and genome architecture. Proteins that associate with RNAPII during transcription elongation play an important role in coupling histone modifications to active transcription. Paf1C, a conserved member of the RNAPII active elongation complex, is required for the ubiquitylation of histone H2B, a modification with effects on nucleosome stability and the methylation and acetylation state of chromatin. Here, we provide insights into how a conserved domain in Paf1C, which we previously showed to be necessary and sufficient for Paf1C-mediated stimulation of H2B ubiquitylation, interacts with the ubiquitin conjugase for H2B thereby guiding its specificity.

This article is a PNAS Direct Submission.

Copyright © 2023 the Author(s). Published by PNAS. This article is distributed under Creative Commons Attribution-NonCommercial-NoDerivatives License 4.0 (CC BY-NC-ND).

[1]T.F. and B.M.M. contributed equally to this work.

[2]Present address: Molecular and Cellular Biology Graduate Program, University of Washington, Seattle, WA 98195.

[3]Present address: Center for Developmental Biology and Regenerative Medicine, Seattle Children's Research Institute, Seattle, WA 98101.

[4]Present address: Department of Biological Sciences, George Washington University, Washington, DC 20052.

[5]Present address: Department of Biology, Ball State University, Muncie, IN 47306.

[6]To whom correspondence may be addressed. Email: arndt@pitt.edu.

This article contains supporting information online at https://www.pnas.org/lookup/suppl/doi:10.1073/pnas.2220041120/-/DCSupplemental.

Published May 22, 2023.

addition, Paf1C is important for coordinating processes coupled to elongation, including transcription termination and RNA 3'-end formation. Importantly, Paf1C also promotes the deposition of several cotranscriptional histone modifications (30). In yeast and other eukaryotes, Paf1C is required for H2BK123 ubiquitylation (31–34) in a manner dependent on a small domain within the Rtf1 subunit, which we termed the histone modification domain (HMD) (33, 35–37). Demonstrating its pivotal role in stimulating H2BK123ub, heterologous expression of the HMD is sufficient to restore H2BK123ub in a yeast strain lacking all five subunits of Paf1C (34). The ability of a recombinant HMD to stimulate H2BK123ub in a reconstituted, transcription-free system argues that Paf1C functions directly in stimulating the ubiquitylation of H2B by Rad6-Bre1 (34). In addition to Rtf1, recent work has shown that other Paf1C subunits contribute to efficient H2B ubiquitylation (34, 38).

The molecular mechanisms underlying how Rad6 and Bre1 specifically target H2B and the role of Paf1C in this process are not fully understood. We previously demonstrated that expression of the HMD outside the context of intact Paf1C restores H2BK123ub levels but leads to mislocalization of the modification, arguing that Paf1C helps control H2BK123ub patterning via tethering the HMD to RNAPII (34). Using site-specific cross-linking, we showed that the HMD directly interacts with Rad6 in vivo and identified the region within the HMD that interacts with Rad6 (34). However, the interaction region within Rad6 remained uncharacterized. The significance of this question is underscored by the multiple functions of Rad6, which, as only one of eleven E2 proteins in budding yeast (39), is targeted to its appropriate substrates through dynamic interactions with other proteins. Here, through site-specific cross-linking and separation of-function mutations, we demonstrate that the N-terminal alpha helix of Rad6 interacts with the HMD and is critical for HMD-mediated stimulation of H2BK123ub. Our findings suggest a highly specific interface between Paf1C and Rad6 that helps direct Rad6 to its nucleosomal substrate.

Results

The Rtf1 HMD Interacts with the N-terminal Alpha Helix of Rad6 In Vitro. Given the dynamic nature of transcription elongation and associated histone modifications, we used a site-specific in vitro cross-linking strategy to identify the region of Rad6 that interacts with the Rtf1 HMD (Fig. 1*A*). Briefly, an engineered tRNA/aminoacyl-tRNA synthetase system and amber codon suppression in *Escherichia coli* were used to express an $HMD_{74–184}$ protein (residues 74 to 184 of Rtf1) with the photoreactive amino acid analogue *p*-benzoyl-L-phenylalanine (BPA) at amino acid 108, replacing a natural phenylalanine at that position (40). Upon photoactivation, BPA cross-links to residues within a 10 Å distance (41). We previously showed that Rtf1-F108BPA cross-linked to Rad6 in vivo and substitution of F108 with alanine greatly diminished cellular levels of H2BK123ub (34). We purified the $HMD_{74\text{-}184\text{-}F108BPA}$ protein (*SI Appendix*, Fig. S1*A*) and showed that it was able to stimulate the levels of H2BK123ub similar to wild-type (WT) HMD in a reconstituted reaction containing recombinant yeast Rad6 (yRad6), yBre1, human E1 (hE1), ubiquitin, and *Xenopus laevis* mononucleosomes (*SI Appendix*, Fig. S1*B*). The $HMD_{74\text{-}184\text{-}F108BPA}$ protein was incubated with recombinant V5-tagged yRad6 alone (Fig. 1*B*) or in the context of a complete H2B ubiquitylation reaction ± ATP (Fig. 1*C* and *SI Appendix*, Fig. S1*C*), and the reaction mixtures were exposed to long-wave ultraviolet (UV) light to activate cross-linking by BPA. In the presence or absence of other factors or catalysis, the $HMD_{74\text{-}184\text{-}F108BPA}$ protein formed a cross-link with Rad6, as detected by western blot analysis when probing for either the HMD (*SI Appendix*, Fig. S1*C*) or Rad6 (Fig. 1 *B* and *C*). Liquid chromatography tandem mass spectrometry (LC-MS/MS) analysis of the V5-Rad6-HMD photocross-linked product, which was gel purified from a reaction containing only V5-Rad6 and $HMD_{74\text{-}184\text{-}F108BPA}$, identified residues in Rad6 that were directly cross-linked to BPA. The highest number of peptide spectral matches mapped to amino acids 9 to 12 in the highly conserved N-terminal alpha helix of Rad6 (Fig. 1 *D* and *E*), although we also detected a small number of cross-links to a C-terminal region of Rad6 and a large number to the N-terminal V5 tag (*SI Appendix*, Table S1). In the absence of additional factors, the HMD–Rad6 interface might be dynamic, explaining the appearance of cross-links to multiple residues. These data demonstrate that Rad6 directly interacts with the Rtf1 HMD in vitro through its highly conserved N-terminal helix and provide a foundation for genetic dissection of this interaction.

Alanine Scanning Mutagenesis Identifies Rad6 Residues Specifically Required for H2BK123ub In Vivo. Guided by our in vitro cross-linking data, we subjected the N-terminal alpha helix of Rad6 to alanine scanning mutagenesis to identify amino acids required for H2BK123ub in yeast. Plasmids expressing WT or mutant derivatives of Rad6 were transformed into a *rad6Δ* strain and histone modifications were assessed by western blotting. Alanine substitutions at positions 10 and 11 of Rad6, which had been identified as $HMD_{74\text{-}184\text{-}F108BPA}$ cross-linking sites (Fig. 1*D*), and also at positions 2, 3, 6, and 8 severely reduced global H2BK123ub levels (Fig. 2*A* and *SI Appendix*, Fig. S2*A*). Levels of H2BK123ub-dependent modifications, namely H3K4me3 and H3K79me2/3, were also reduced in these mutants (Fig. 2*A*). Substitutions at positions 9, 12, and 13 of Rad6 caused a more modest reduction in H2BK123ub levels (Fig. 2*A* and *SI Appendix*, Fig. S2*A*). In all *rad6* substitution mutants, Rad6, Bre1, and Rtf1 levels were similar to WT levels, arguing that the loss of H2BK123ub is not due to decreased levels of these important H2B ubiquitylation factors (Fig. 2*A* and *SI Appendix*, Fig. S2*B*).

To determine if the *rad6* mutants exhibit phenotypes associated with the loss of H2BK123ub specifically or if they are more broadly impaired in Rad6 functions, we performed a set of phenotypic tests. Consistent with the requirement for H2BK123ub in the silencing of genes positioned near telomeres (9), the *rad6* mutants that have the greatest defects in H2BK123ub (substitutions S2A, T3A, R6A, R8A, M10A, and R11A) are all defective in silencing a *URA3* reporter gene positioned near a telomere (Fig. 2*B*). These mutants are strongly sensitive to media containing 5FOA, a compound that is toxic to *URA3*-expressing yeast cells, while mutants with WT levels of H2BK123ub (P4A, R7A, and K14A) grow normally on this media (Fig. 2*B*). Mutants with intermediate defects in H2BK123ub (L9A, D12A, and F13A) show only a modest reduction in growth (Fig. 2*B*).

In contrast to the strong correlation between telomeric silencing and H2BK123ub defects, only one *rad6* substitution mutant, *rad6-R8A*, was strongly sensitive to UV irradiation, a phenotype that reflects the ability of Rad6 to modify proliferating cell nuclear antigen (PCNA) and promote DNA damage repair via translesion synthesis (Fig. 2*C*) (23). One other mutant, *rad6-D12A*, was sensitive to the highest dose of UV exposure, but none of the other H2BK123ub-defective *rad6* mutants shared this property. Another well-established process dependent on Rad6 is proteolysis of substrates through the N-degron pathway (24, 25). To test for defects in N-degron pathway function in the *rad6* mutants, we used a

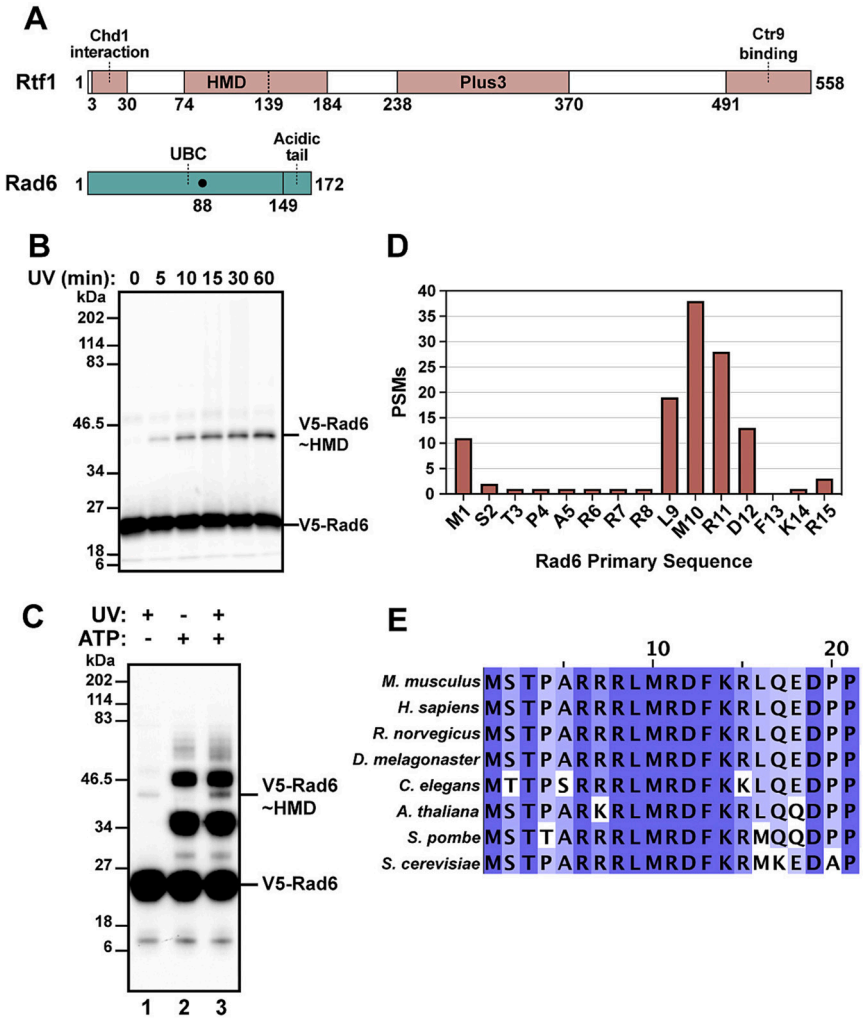

Fig. 1. In vitro site-specific cross-linking identifies a conserved HMD-interacting region within the Rad6 N terminus. (*A*) Protein domain architecture of yeast Rtf1 and Rad6. The schematics show structurally and/or functionally characterized domains. *Top*: Chd1 interaction, HMD, Plus3, and Ctr9 binding domains of Rtf1 are shown (34, 35, 38, 42, 43). The dotted line within the HMD of Rtf1 defines the minimal region (residues 74 to 139; $HMD_{74\text{-}139}$) necessary and sufficient for H2BK123ub in vivo (34). Rtf1 Residues 74 to 184 ($HMD_{74\text{-}184}$) correspond to the larger region required for in vitro stimulation of H2BK123ub using recombinant HMD (34). *Bottom*: the ubiquitin conjugating enzyme (UBC) and the acidic tail domains of Rad6 are shown (44). Rad6 catalytic cysteine (C88) is indicated by a black dot within the UBC domain. (*B*) Recombinant V5-Rad6 and $HMD_{74\text{-}184\text{-}F108BPA}$ were mixed and exposed to UV light (365 nm) for the indicated periods of time. Cross-linking was monitored by western blot analysis using anti-V5 antibody. (*C*) Western blot probed with anti-V5 antibody to detect cross-linked products in a complete H2B ubiquitylation reaction containing V5-Rad6, $HMD_{74\text{-}184\text{-}F108BPA}$, yBre1, ubiquitin, hE1, and *X. laevis* nucleosomes with or without ATP. Reactions were exposed to UV light as indicated. Lane 1 lacked ATP and contained apyrase. The ATP-dependent high molecular weight V5-reactive species are likely ubiquitylated forms of V5-Rad6. (*D*) Mass spectrometry analysis of cross-linked V5-Rad6~$HMD_{74\text{-}184\text{-}F108BPA}$, quantified as peptide spectrum matches (PSMs), identifies residues in the N-terminal helix of Rad6 that cross-linked to the HMD in vitro. (*E*) Multiple sequence alignment of the Rad6 N-terminal region. A darker color indicates higher conservation across species. This panel was generated using Jalview (45).

well-characterized plasmid-based reporter expressing an unstable substrate: β-galactosidase with a strongly destabilizing amino acid, Arg, at the N-terminal position (46). Degradation of this substrate is dependent on Rad6 and the E3 Ubr1 (24, 25, 47) (Fig. 2*D*). In contrast to *rad6Δ* and *ubr1Δ* strains and when compared to WT, the single alanine substitutions caused little if any effect on the levels of the N-degron substrate, as measured by β-galactosidase assays in extracts from the mutants (Fig. 2*D*). Finally, a recent study demonstrated a role for Rad6 in the cellular response to oxidative stress through ubiquitylation of ribosomal proteins (27). Exposure of yeast cells to hydrogen peroxide revealed strong sensitivity for the *rad6Δ* mutant, modest sensitivity for the *rad6-R8A* mutant, and WT levels of resistance for the other mutants (*SI Appendix*, Fig. S2*C*). As summarized in *SI Appendix*, Fig. S2*D*, our genetic analysis of the Rad6 N-terminal helix has identified mutations that impair H2BK123ub and processes requiring this mark but apparently do not affect three other Rad6-dependent pathways.

Separation-of-Function Mutations Identify Rad6 Residues Required for Stimulation by the HMD. The lack of H2BK123ub in the *rad6* mutants could arise through multiple mechanisms, including disrupted binding of Rad6 to the HMD, Bre1, nucleosomes, or other factors. Therefore, to specifically test the ability of the Rad6 substitution mutants to respond to stimulation by the HMD, we turned to the in vitro H2B ubiquitylation assay assembled with recombinant factors. For these experiments, we purified WT and mutant Rad6 proteins (*SI Appendix*, Fig. S3*A*); each of the nine mutants selected was defective for H2BK123ub in vivo (Fig. 2*A* and *SI Appendix*, Fig. S2*A*).

In agreement with our prior work (34), recombinant $HMD_{74\text{–}184}$ can stimulate the level of Bre1-dependent H2BK123ub in the reconstituted reaction approximately threefold (Fig. 3 *A* and *B*, compare hatched and red bars in B). The Rad6 mutants fell into three groups. In the first group, the R8A and R11A mutants are strongly defective for H2BK123ub in vitro even in the basal condition, defined as in the presence of Bre1 but not HMD (Fig. 3

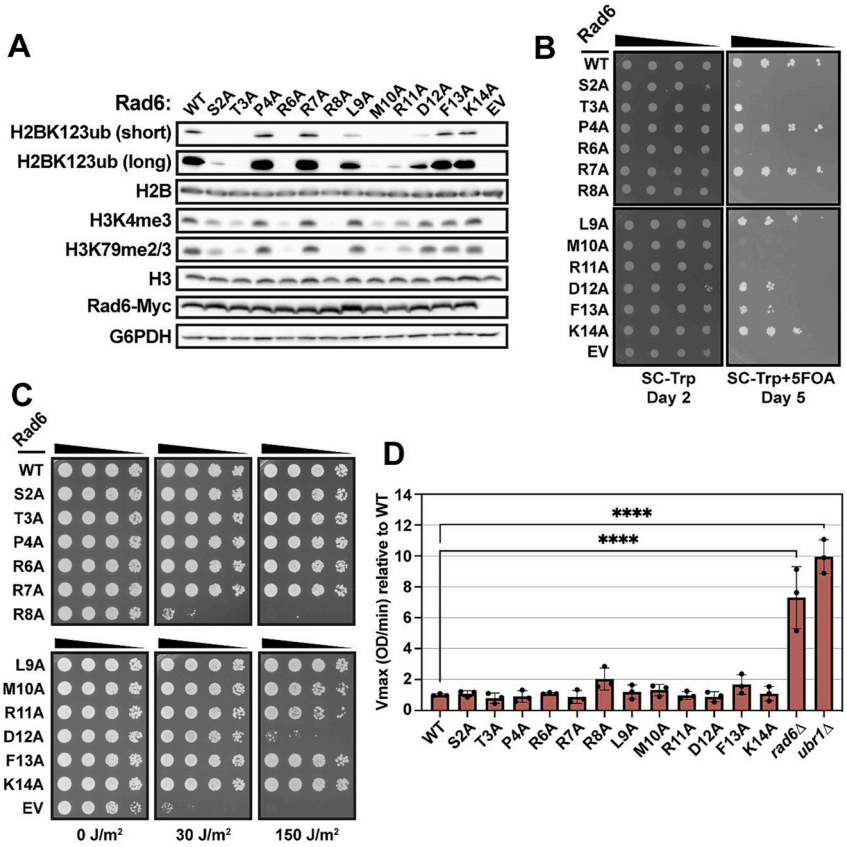

Fig. 2. Alanine scanning mutagenesis of Rad6 N-terminal helix identifies residues required for H2B ubiquitylation. (*A*) A *rad6Δ* strain (KY2045) was transformed with plasmids expressing WT *RAD6* or *rad6* mutant alleles, and extracts of transformants were analyzed by western blotting with antibodies against the indicated proteins. Short and long exposures of the same H2BK123ub blot are shown. EV = empty vector. G6PDH serves as a loading control. (*B*) A *rad6Δ* strain (KY3391) bearing a telomeric silencing reporter (*TELVR::URA3)* was transformed with WT or mutant *rad6* plasmids, and transformants were spotted in a fivefold serial dilution series onto SC-Trp+5FOA or growth control media (SC-Trp). (*C*) Fivefold serial dilution spot assay of KY2045 transformants followed by exposure to indicated doses of UV irradiation. Representative images show growth on day two relative to the time of plating. (*D*) Function of alanine-substituted *rad6* mutants in protein degradation via the N-degron pathway was assayed using a β-galactosidase reporter with a destabilizing residue (Arg) at the N terminus (46). Relative V_{max} values for β-galactosidase were calculated with reference to the average V_{max} from the WT measurements. All strains were assayed in biological triplicate and technical duplicate. Transformants of strain KY3392 contained two plasmids: the Arg-β-galactosidase reporter (pKB1526) and a WT or mutant *rad6* plasmid. The *ubr1Δ* control strain was constructed by transforming the WT *RAD6* plasmid (pKB1167) into a *rad6Δ ubr1Δ strain* (KY3389). Mean and SD are shown. Significant differences compared to the WT are indicated by asterisks based on an unpaired one-way ANOVA with Dunnett's post hoc test (****$P < 0.0001$).

A and *B* and *SI Appendix*, Fig. S3*B*). For R8A, this strong defect correlates with phenotypes in addition to the loss of H2BK123ub and telomeric silencing, including UV sensitivity on par with the *rad6Δ* mutant (Fig. 2*C*) and moderate sensitivity to hydrogen peroxide (*SI Appendix*, Fig. S2*C*). Within the structure of Rad6, R8 is engaged in a network of interactions that likely contribute to the structural fold (44). The behavior of the R11A mutant appears more specific to H2BK123ub and a lack of response to Bre1 (*SI Appendix*, Fig. S3*B*), as this mutant confers a strong H2BK123ub defect yet supports WT levels of N-degron activity and tolerance to UV and oxidative stress (Fig. 2 and *SI Appendix*, Fig. S2). In the second group, mutants S2A and T3A surprisingly behaved like WT Rad6 in vitro despite their severe effect on H2BK123ub in vivo (Fig. 2*A* and *SI Appendix*, Fig. S2*A*). This suggests that Rad6 residues S2 and T3 are required for a step in H2B ubiquitylation that manifests in vivo, possibly for the response to other factors like Lge1 (20, 48). In the third group, the Rad6 R6A, L9A, M10A, D12A, and F13A mutant proteins all show reduced ability to be stimulated by the HMD (Fig. 3*B*, red bars) yet support near WT or even greater (D12A) levels of H2BK123ub in the absence of the HMD (Fig. 3*B*, hatched bars).

With respect to fold stimulation by the HMD, the R6A and M10A mutants are the most strongly affected. Interestingly, M10 was the primary site of cross-linking between the $HMD_{74\text{-}184\text{-}F108BPA}$ protein and Rad6 in vitro (Fig. 1*D*).

Using published structures (34, 44) and instructed by our in vitro BPA cross-linking results, we generated a model of the putative Rad6–HMD interface using ClusPro 2.0 (Fig. 3*C*) (*SI Appendix*, *Materials and Methods*). This model positions R6 and M10 of Rad6 near HMD residues that cross-link to Rad6 in vivo (Rtf1 T105, F108, Q112) (34) and in vitro (Rtf1 F108; Fig. 1). In addition, we used AlphaFold-Multimer (49, 50) to generate a model of the Rad6–HMD interaction independent of experimental constraints (*SI Appendix*, Fig. S3*C*). Remarkably, the AlphaFold-Multimer prediction also places the Rad6 M10 residue in close proximity to Rtf1 F108 and other residues that cross-link to Rad6 in vivo (34). Despite this striking similarity, the two models differ in the orientation of Rad6 relative to the HMD. Essentially, the two predictions differ by an approximately 180° rotation of Rad6 relative to the HMD centered on an interaction point containing Rad6 M10, Rtf1 F108 and adjacent residues. To begin testing the interface proposed by both in silico models, we incorporated BPA into Rad6, replacing amino acids P4, R7, or F13 via amber codon suppression in yeast (51). Alanine substitutions of these amino acids caused minor, if any, effects on H2BK123ub in vivo (Fig. 2*A* and *SI Appendix*, Fig. S2*A*). Yeast transformants harboring the tRNA/aminoacyl-tRNA synthetase plasmid for BPA incorporation and a plasmid containing either WT *RAD6* or an amber codon derivative of *RAD6* were grown in BPA-containing media and exposed to long-wave UV light. Consistent with both in silico models, which place Rad6 F13

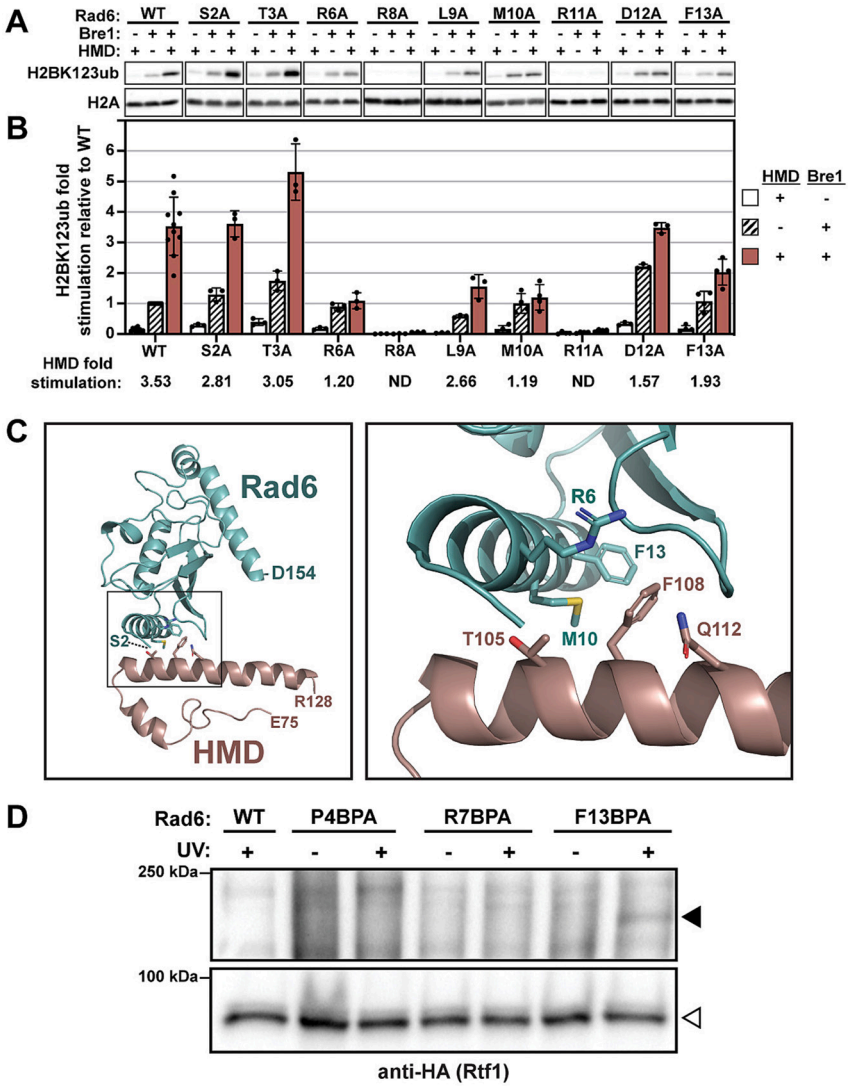

Fig. 3. Specific residues in the Rad6 N terminus are required for stimulation of H2BK123 ubiquitylation by the HMD in vitro. (*A*) Representative western blots show the extent of H2BK123 ubiquitylation in the absence of either $HMD_{74–184}$ or yBre1 or in the presence of both. H2A serves as the loading control. (*B*) Quantification of western blots shown in *A*. Unfilled (white) bars represent reactions containing the HMD but lacking Bre1. Hatched bars represent reactions containing Bre1 but lacking the HMD. Red solid bars represent reactions containing both Bre1 and the HMD. H2BK123ub fold stimulation in all lanes was calculated relative to H2BK123ub-normalized signal from WT Rad6 in the presence of Bre1 and absence of the HMD (WT middle lane) (*SI Appendix, Materials and Methods*). Points show individual measurements (minimum of three technical replicates). Mean and SD are shown. Below the graph, H2BK123ub-normalized signals in both Bre1-containing reactions were used to calculate the HMD fold stimulation per mutant as the ratio between H2BK123ub in the presence and absence of the HMD. ND = not determined due to very low signals. (*C*) Cross-linking-instructed model of the Rad6–HMD interface using crystal structures of Rad6 (PDB ID: 1AYZ) and Rtf1 HMD (PDB ID: 5E8B). Docking was done using ClusPro 2.0. The *Inset* in the left panel is expanded on the right. (*D*) In vivo BPA cross-linking followed by western blot analysis with antibody against the 3×HA tag on Rtf1 shows the appearance of a UV-dependent cross-linked species when Rad6-F13 is substituted with BPA in yeast. A *rad6Δ* strain (KY2798) was cotransformed with a plasmid encoding the tRNA/aminoacyl-tRNA synthetase and a 2μ plasmid expressing either WT *RAD6* or *rad6* amber codon mutations, allowing BPA incorporation at the indicated locations in Rad6. Black arrowhead denotes the Rad6~3×HA-Rtf1 cross-linked product. White arrowhead indicates levels of uncross-linked 3×HA-Rtf1.

near the interface with the HMD, the Rad6-F13BPA derivative reproducibly cross-linked to 3×HA-Rtf1, as assessed by western blotting (Fig. 3*D*). While additional experiments, such as structural studies that include Bre1 and the nucleosome substrate, will be needed to differentiate between the two predictive models, our in vivo cross-linking results independently support our in vitro cross-linking, biochemical, and genetic data on the Rad6-HMD interaction.

Targeted *rad6* Mutations Specifically Disrupt HMD-Dependent H2BK123 Ubiquitylation. Based on our molecular models and analysis of single substitution mutants, we hypothesized that Rad6 amino acids R6 and M10 are particularly important for the Rad6–HMD interaction. To uncover the effects of *rad6-R6A* and *rad6-M10A* on H2B ubiquitylation in vivo with greater sensitivity, we deleted *UBP8* and *UBP10*, the genes encoding the deubiquitylases that target H2BK123ub (3). Unlike results observed in the presence of *UBP8* and *UBP10* (Fig. 4*A*, left), deletion of these genes revealed residual H2BK123ub and higher levels of H3K4me3 and H3K79me2/3 in the *rad6-R6A*, *rad6-R8A* and *rad6-M10A* mutants indicating that they are hypomorphic for H2BK123ub loss (Fig. 4*A*, right).

To generate *rad6* mutants more severely compromised for HMD-mediated stimulation of H2BK123ub, we constructed a *rad6-R6A, M10A* double mutant and also a *rad6-R6Q* mutant. The latter was chosen based on surveying human cancer databases (COSMIC, ClinVar, and NCBI dbSNP) to identify recurring missense mutations in the N-terminal region of either UBE2A or

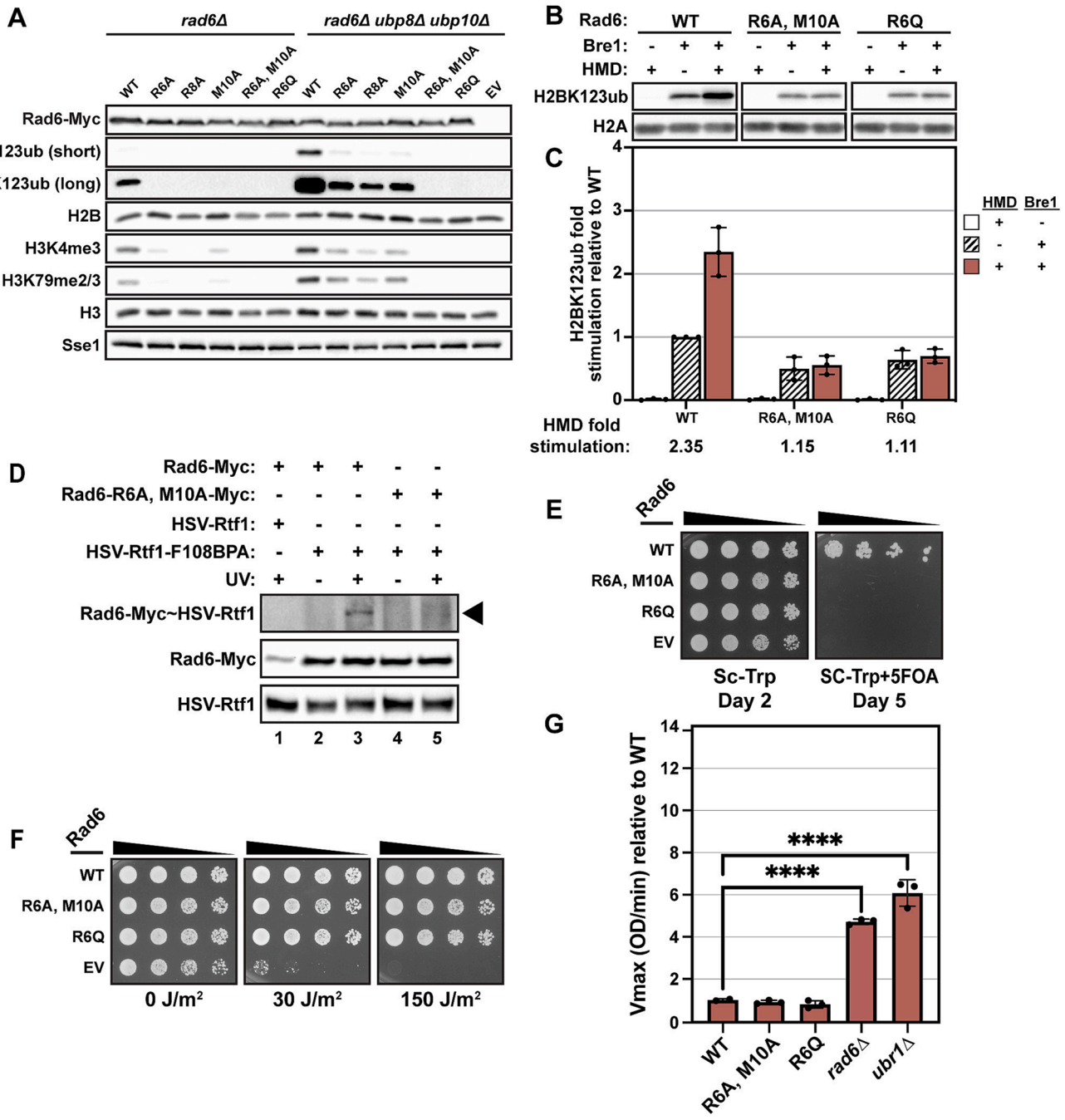

Fig. 4. *rad6-R6Q* and *rad6-R6A, M10A* mutants are severely and specifically defective in the H2BK123ub pathway. (*A*) Either *rad6Δ* (KY2045) or *rad6Δ ubp8Δ ubp10Δ* (KY4010) strains were transformed with WT or *rad6* mutant plasmids followed by western blot analysis. Sse1 serves as a loading control. Short and long exposures of the same H2BK123ub blot are shown. EV = empty vector. (*B* and *C*) In vitro H2B ubiquitylation assay and associated quantitation (as in Fig. 3 *A* and *B*) to assess the basal activity and response of Rad6-R6A, M10A and Rad6-R6Q proteins to HMD stimulation. (*D*) In vivo BPA cross-linking followed by western blot analysis with antibodies against the HSV tag on 3×HSV-Rtf1 or the Myc tag on Rad6-13xMyc. As indicated, *rtf1Δ RAD6 (KY2507) and rtf1Δ rad6-R6A, M10A (KY4389)* strains were cotransformed with a 2μ plasmid expressing WT *3xHSV-RTF1* or a derivative of this plasmid with an amber codon at position 108 along with the tRNA/aminoacyl-tRNA synthetase plasmid for BPA incorporation. Samples were loaded such that equal amounts of full-length Rtf1 were present in each lane. The arrowhead denotes the Rad6-Myc~HSV-Rtf1 cross-linked product detected using anti-Myc antibody. (*E*) Fivefold serial dilution spot assay of *rad6Δ TELVR::URA3* (KY3391) transformants similar to Fig. 2*B*. (*F*) Fivefold serial dilution spot assay of *rad6Δ* (KY2045) transformants on SC-Trp medium followed by exposure to indicated doses of UV irradiation. Representative images show growth on day two relative to the time of plating. (*G*) Protein degradation via the N-degron pathway was assayed as in Fig. 2*D* except that WT was measured in biological duplicate with one assayed in technical quadruplicate and the other in duplicate. Mean and SD are shown. Significant differences compared to the WT are indicated by asterisks based on an unpaired one-way ANOVA with Dunnett's post hoc test (****$P < 0.0001$).

UBE2B, the human homologs of yeast Rad6. Strikingly, the *rad6-R6Q* and *rad6-R6A, M10A* mutants lack detectable H2BK123ub, H3K4me3 and H3K79me2/3 either in the presence or absence of *UBP8* and *UBP10* (Fig. 4*A* and *SI Appendix*, Fig. S4*A*). Protein levels of Rad6, Bre1, and Rtf1 in all strains were similar to WT (*SI Appendix*, Fig. S4*B*).

To test if the R6Q and R6A, M10A substitutions disrupt the response of Rad6 to the HMD, we purified Rad6-R6A, M10A and Rad6-R6Q proteins (*SI Appendix*, Fig. S4*C*) and tested their activity in the reconstituted H2B ubiquitylation assay. Both mutant proteins were severely defective in responding to the HMD yet retained significant basal activity albeit at a lower level

than WT (Fig. 4 *B* and *C*, compare hatched to red bars; and *SI Appendix*, Fig. S4*D*). Additionally, we tested if the *rad6-R6A, M10A* mutation disrupted the interaction between Rad6 and Rtf1 in vivo using BPA cross-linking (Fig. 4*D*). Western blots show that the cross-linking of Rtf1-F108BPA to Rad6-R6A, M10A was markedly reduced compared to that observed with WT Rad6 (Fig. 4*D*, compare lanes 3 and 5). In agreement with these results and the severe loss of global H2BK123ub (Fig. 4*A*), the *rad6-R6Q* and *rad6-R6A, M10A* mutants exhibit a telomeric silencing defect (Fig. 4*E*). However, when examined for UV sensitivity (Fig. 4*F*), N-degron defects (Fig. 4*G*), and tolerance to oxidative stress (*SI Appendix*, Fig. S4*E*), both mutants appear nearly indistinguishable from WT. Finally, given the reported links between H2BK123ub and DNA repair (52), we wanted to determine the level of UV sensitivity that could be ascribed to loss of H2BK123ub. Accordingly, we tested the UV sensitivity of strains containing genomic mutations in different H2B K123 ubiquitylation factors (*SI Appendix*, Fig. S4*F*). This group included *rad18Δ* and *rad6Δ* strains as a reference for high sensitivity to UV (53). In addition to *rad6-R6Q* and *rad6-R6A, M10A* mutants, we tested a strain deleted for *BRE1*, a strain expressing H2B-K123R from both H2B-encoding genes (*htb1-K123R htb2-K123R*), and an *rtf1-108-110-AAA* strain, which contains a triple amino acid substitution within the HMD (37) at the position of cross-linking with Rad6 (34). Compared to *rad6Δ* and *rad18Δ*, none of the other H2BK123ub-defective mutants show comparable levels of UV sensitivity (*SI Appendix*, Fig. S4*F*). Collectively, our results highlight the key contributions of specific amino acids within the Rad6 N-terminal helix to a functional Rad6–HMD interface and H2BK123 ubiquitylation.

Extensive Overlap between the Transcriptomes of *rad6* and HMD Point Mutants. To more comprehensively assess the extent to which the *rad6-R6A, M10A* and *rad6-R6Q* mutants are specific to the H2BK123ub pathway, we utilized RNA sequencing (RNA-seq) as a sensitive phenotyping method. RNA-seq was performed on rRNA-depleted steady-state RNA from WT control strains and a set of integrated mutants: *rad6Δ*, H2B-K123R, *rtf1-108-110-AAA*, *rad6-R6Q,* and *rad6-R6A, M10A. Kluyveromyces lactis* was used as a spike-in control for data normalization (*SI Appendix*, *Materials and Methods*). We hypothesized that if the proposed Rad6–HMD interaction interface is specific to the H2BK123ub pathway, then mutating residues on either side of the interface will yield highly similar effects on the transcriptome, which will also phenocopy an H2B-K123R mutant.

All mutants except the H2B-K123R strain bear a 13×Myc C-terminal tag on *RAD6* and a 3×HA N-terminal tag on *RTF1.* Therefore, RNA-seq was performed on two WT strains (*RAD6 RTF1* and *RAD6-13xMyc 3x-HA-RTF1*) and two *rad6Δ* strains (*rad6Δ RTF1* and *rad6Δ 3xHA-RTF1*) to provide matched WT references for appropriate experimental samples and identify any tag effects. For all strains, results obtained from three biological replicates were highly reproducible (*SI Appendix*, Fig. S5*A*). Differential expression analysis using DEseq2 (54) was performed on transcripts separately mapped to either the sense or antisense strands of coding regions. Principal component analysis (PCA) of the RNA-seq results showed WT strains clustering the furthest from *rad6Δ* strains with reference to PC1, while other H2BK123ub-defective mutants grouped between the two extremes (*SI Appendix*, Fig. S5*B*). Comparisons between the two WT strains or the two *rad6Δ* strains revealed that less than 1% of all transcripts were differentially regulated due to the tags on *RAD6* and/or *RTF1* (*P*-adjusted ≤ 0.05) (*SI Appendix*, Fig. S5*C*). Nevertheless, the comparison of WT strains revealed slight background differences within a narrow fold-change range and above the *P*-adjusted value 0.05 (*SI Appendix*, Fig. S5*C*). Overall, these results justify further direct comparisons between the mutants.

Relative to their respective WT, all mutants displayed a large number of differentially expressed sense and antisense transcripts (Fig. 5 *A* and *B*, top rows). The observed increase in antisense transcripts among the H2BK123ub-defective mutants is in agreement with reports of increased antisense transcription in *Schizosaccharomyces pombe* H2B ubiquitylation mutants (8, 55), although to our knowledge this is the first time this effect has been reported for an *S. cerevisiae* integrated H2B-K123R double mutant. To assess the extent of overlap between their transcriptomes, we next performed direct mutant-to-mutant comparisons (Fig. 5 *A* and *B*, bottom rows). Comparisons of the *rad6-R6A, M10A* and *rad6-R6Q* mutants to each other or to the *rtf1-108-110-AAA* mutant revealed almost no differences in either the sense or antisense direction (Fig. 5 *A* and *B*, bottom rows and *SI Appendix*, Fig. S5*D*). In contrast, direct comparisons of the *rad6-R6A, M10A* or *rad6-R6Q* transcriptomes to the *rad6Δ* transcriptome revealed hundreds of differentially expressed sense transcripts that passed the statistical cutoff, with 16% of these falling outside a log2 fold-change range of −1 to +1 (Fig. 5 *A*, *Bottom* and *SI Appendix*, Fig. S5 *D*, *Top*). Collectively, these mutant comparisons strongly support the high specificity of the *rad6-R6A, M10A* and *rad6-R6Q* point mutations for the Rad6–HMD interaction.

When viewed as a Venn diagram, extensive overlap is also apparent among the differentially regulated sense transcripts in the *rad6* and *rtf1* point mutants relative to their WT controls (Fig. 5*C*). Consistent with the direct mutant-to-mutant comparisons, these genes represent only a subset of the differentially expressed genes observed in the *rad6Δ* strain. As expected, given the importance of the HMD–Rad6 interaction for H2B ubiquitylation, the transcriptome of the H2B-K123R mutant largely overlapped with the transcriptomes of the other mutants. However, this analysis also revealed differentially expressed transcripts unique to the H2B-K123R mutant. Although these transcriptional differences might reflect ubiquitylation-independent functions of K123, they appear to be dominated by small effects and more than 94% of them in the mutant-to-mutant comparisons are within a log2 fold-change range of −1 to +1 (Fig. 5 *A* and *B*, *Bottom*; *SI Appendix*, Fig. S5*D*). Finally, hierarchical clustering based on differentially expressed sense transcripts highlights the close relationship among all three interface mutants and their distinction from the *rad6Δ* mutant (Fig. 5*D*). Overall, our RNA-seq results circumvent the limitations posed by single-phenotype tests and strengthen our conclusion that specific substitutions in the Rad6 N-terminal helix uniquely impair the functional interaction between Rad6 and the HMD.

Discussion

In this study, we showed that the N-terminal helix of Rad6 is critical for its interaction with the Rtf1 subunit of Paf1C and for ubiquitylation of H2BK123, a conserved modification that broadly impacts chromatin structure, transcription, and a cascade of histone modifications. Our previous site-specific cross-linking experiments with BPA-substituted Rtf1 revealed a direct interaction between Rad6 and the HMD in vivo (34). Here, through site-specific cross-linking, genetic analysis, and in vitro H2B ubiquitylation assays, we identified Rad6 residues R6 and M10 as being especially important for and specific to the Rad6–HMD interaction. In support of this conclusion, mutation of either side

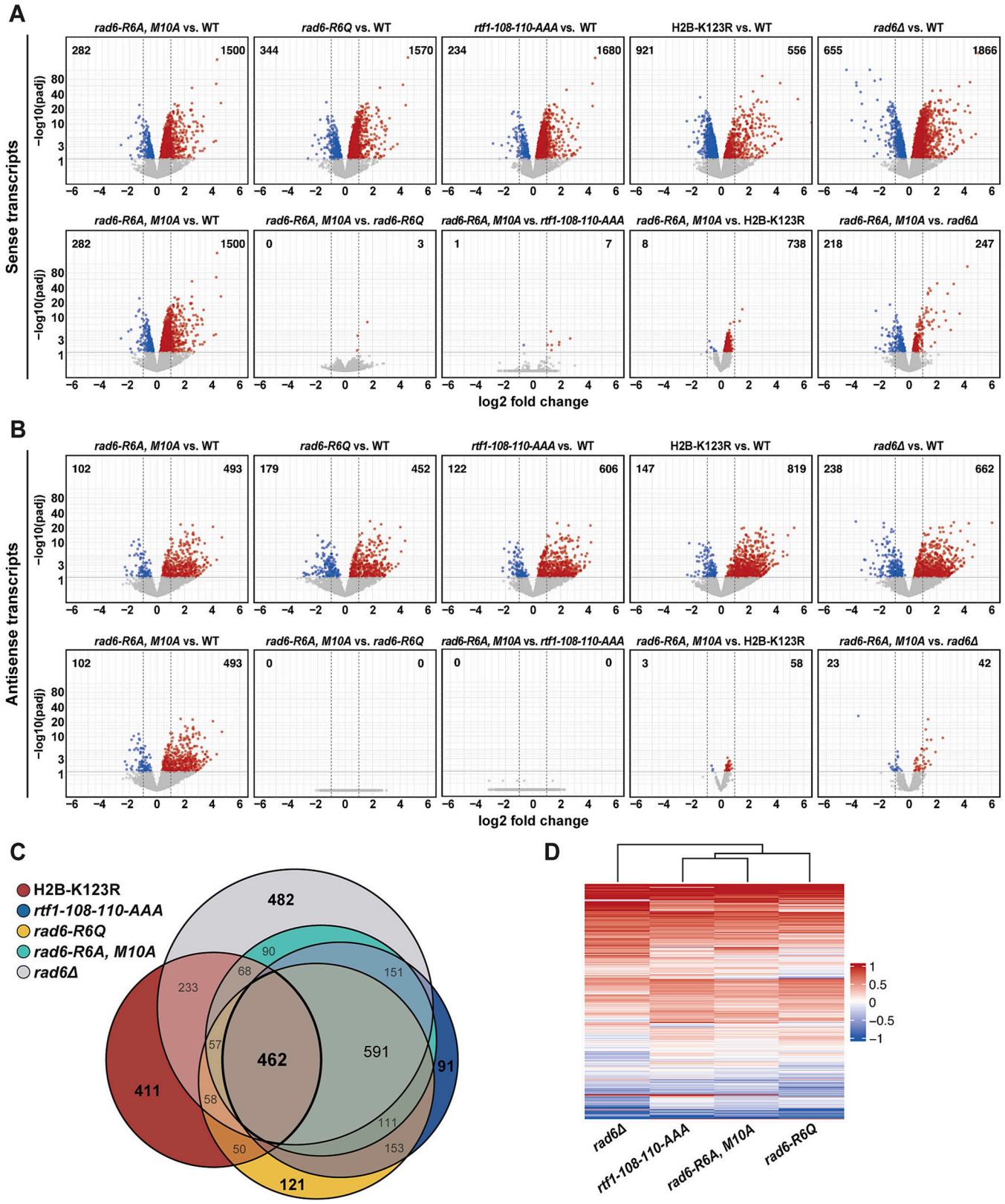

Fig. 5. *rad6-R6A, M10A* and *rad6-R6Q* mutants phenocopy H2BK123ub-deficient mutants at the transcriptome level. (*A*) *Top*: Volcano plots displaying the differential expression analysis of sense transcripts in each mutant with respect to its corresponding WT control. All mutants were compared to the *3xHA-RTF1 RAD6-13xMyc* WT (i.e., tagged WT) except H2B-K123R, which was compared to the *RAD6 RTF1* WT (i.e., untagged WT). The *rad6Δ* mutant shown far right corresponds to the *rad6Δ 3xHA-RTF1* strain. The numbers of genes that pass the 0.05 *P*-adjusted value threshold whether up- (red) or down-regulated (blue) are shown at the top corners of each volcano plot. *Bottom*: Volcano plots of mutant-to-mutant comparisons. *rad6-R6A, M10A* was compared to the tagged WT and all the other mutants to emphasize the differences among the strains. Dashed vertical lines indicate the −1 to +1 range of log2 fold changes. Horizontal cutoff line represents the 0.05 *P*-adjusted (padj) value. (*B*) Same analysis as in *A* but based on the antisense transcripts only. (*C*) Venn diagram showing the overlap in the sets of differentially regulated sense transcripts (up and down) in each mutant relative to its corresponding WT. A significance threshold of *P*-adjusted value ≤ 0.05 was used. (*D*) Heatmap showing hierarchical clustering of the indicated mutant strains based on the log2-fold change values of the sense transcripts in the mutants with reference to WT.

of the proposed Rad6–HMD interface yielded strikingly similar transcriptomic profiles that were distinct from those of a *rad6Δ* strain. Our findings provide mechanistic insights underlying Paf1C-stimulated cotranscriptional ubiquitylation of H2B.

The N-terminal helix of Rad6 is highly conserved and has been implicated in multiple Rad6 functions. Although it does not eliminate nuclear localization or charging by the E1 in vitro, a mutation that deletes the N terminus of Rad6 (*rad6Δ 1-9*) causes defects in the N-degron pathway and interaction with Ubr1, H2BK123ub and downstream H3 methylation, telomeric silencing, Ty1 element transposition, and UV tolerance (9, 22, 53, 56). Our mutational studies identified specific amino acid substitutions in the Rad6 N-terminal helix that cause a range of H2BK123ub and telomeric silencing defects yet have little effect on UV sensitivity, N-degron protein degradation, or response to oxidative stress. One possible explanation for our results considering the pleiotropic effects of the *rad6Δ 1-9* mutation is that the HMD–Rad6 interaction, and hence H2BK123ub, is particularly sensitive to the integrity of the Rad6 N-terminal helix. Other proteins that require an intact Rad6 N-terminal helix for their functions might interact with other regions of Rad6 and, therefore, are relatively resistant to the effects of single amino acid substitutions in the N-terminal helix. Notable among the substitutions we identified in our screen are Rad6-R6A, M10A and Rad6-R6Q, a cancer-associated change, which severely reduce deposition of H2BK123ub in vivo and stimulation by the HMD in vitro. Consistent with our results, a previous genetic screen identified a double mutant (*rad6-P4L, A5V*) that was partially defective in telomeric silencing but not N-degron function or UV tolerance (56), although the mechanistic basis for the loss of telomeric silencing was undefined. The requirement of the N-terminal helix for various Rad6 functions, together with our identification of N-terminal mutants that are specifically defective in H2BK123ub and stimulation by the HMD, suggests that this helix serves as a hub for multiple Rad6 binding partners.

Reported interactions involving the Rad6 N-terminal helix include interactions with Uba1 (E1) and Ubr1, the E3 for N-degron proteolysis (27, 53, 57, 58). Rad6 R7, R8 and R11 constitute an E1 binding motif that is conserved among E2 proteins (58, 59). In the Rad6 structure, R8 is engaged in intramolecular hydrogen bonding that stabilizes the structural fold (44). Our in vitro data showing near complete loss of basal H2B ubiquitylation activity for the Rad6-R8A and Rad6-R11A mutant proteins are consistent with the involvement of these residues in protein stability and/or E1 binding. However, because $Rad6_{\Delta 1\text{-}9}$ can be charged by the E1 in vitro (53), residues distal to the Rad6 N-terminal region must also contribute to the Rad6–E1 interaction (58). Unlike *rad6-R8A*, which is hypomorphic for many of the phenotypes tested (*SI Appendix*, Fig. S2*D*), *rad6-R11A* appears to be selectively defective in H2BK123ub, suggesting this residue functionally or physically interacts with a key member of the H2B ubiquitylation machinery, possibly Bre1 (*SI Appendix*, Fig. S3*B*). Recent cryo-electron microscopy structures show that Rad6 R6 is part of an extensive interaction interface (823.3 $Å^2$) with Ubr1 (57). In the N-degron assay used here, the *rad6-R6A*, *rad6-R6Q,* and *rad6-R6A, M10A* mutants behave similar to WT, arguing that substitution of R6 alone is insufficient to severely compromise the interaction with Ubr1. In the context of existing literature, our data suggest that residues R6 and M10 are unlikely to confer strong effects on Rad6 binding to the E1 or Ubr1, although they might contribute to such interactions.

The striking similarities among the HMD (*rtf1-108-110-AAA)* and Rad6 interface mutants (*rad6-R6Q* and *rad6-R6A, M10A*) on the transcriptome level, together with the phenotypic and transcriptomic distinction of these mutants from the *rad6Δ* strain, are indicative of the specificity of this interface for H2BK123ub. Consistent with this conclusion, the transcriptomic profile of the H2B-K123R mutant largely overlapped with those of the other mutants. We also observed an independent subset of transcripts specific to the H2B-K123R mutant, which might reflect loss of ubiquitylation-independent functions of K123 such as its role as a site for histone acetylation (60, 61). However, we cannot rule out that some of the deviation between the transcriptomic profiles among the mutants might stem from slight variation imposed by tagged alleles and/or spike-in normalization (*SI Appendix*, Fig. S5 *A–C*).

Although other contact points between Rad6 and Rtf1 might contribute, we believe that the Rad6–HMD interface proposed here is critical in targeting Rad6 to its histone substrate during transcription elongation. This likely happens in coordination with other Rad6-Paf1C contacts, including recently reported biochemical interactions of Rad6 with Ctr9 and Cdc73 (38). Additionally, Cdc73 and Rtf1, in an HMD-dependent manner, can accelerate ubiquitin discharge from Rad6 independently and in coordination with Bre1 in vitro (38). In light of other reported interactions between Bre1 and Rad6 (62–65), Bre1 and the nucleosome (63), Bre1 and Paf1C (32), and the HMD and the nucleosome (66), it is evident that cotranscriptional H2B ubiquitylation is the product of a complex process entailing multivalent interactions. Future work is required to address the mechanistic and structural aspects that pose a critical requirement for the proposed Rad6–HMD interface and to pinpoint the order of events leading to efficient cotranscriptional H2B ubiquitylation in vivo.

Materials and Methods

Yeast strains used in this study are derived from S288C (67) and listed in *SI Appendix*, Table S2, and plasmids are described in *SI Appendix*, Table S3. Yeast cell extracts were made using a slightly modified NaOH extraction method (68), except for extracts in (Figs. 3*D* and 4*D*) that were made by trichloroacetic acid extraction as previously described (34). Proteins were resolved using sodium dodecyl sulfate (SDS)-polyacrylamide gel electrophoresis followed by immunoblotting. In vivo BPA cross-linking and in vitro H2B ubiquitylation reactions were done essentially as described (34). Additional information and description of the statistical analysis and reproducibility is described in the *SI Appendix* (*SI Appendix, Materials and Methods*).

In Vitro BPA Cross-Linking. For in vitro cross-linking followed by western blot analysis, BPA cross-linking of purified proteins was performed in conditions identical to the in vitro ubiquitylation reactions, except in Fig. 1*C* lane 1 and *SI Appendix*, Fig. S1*C* lane 1 where buffer lacked adenosine triphosphate (ATP) and contained 0.02 units of apyrase (Sigma A6535). Reaction mixtures were incubated for 10 min at 30 °C before performing the cross-linking at 4 °C for 30 min using long-wave UV light (365 nm). A UVGL-55 handheld UV lamp was placed ~3 cm on top of the reaction mixture, which was dropped onto parafilm. The reaction mixture was then boiled in SDS loading buffer and run on a 12% SDS-polyacrylamide gel. For LC-MS/MS analysis, reactions contained 37 µg $HMD_{74\text{-}184\text{-}F108BPA}$ and 16.25 µg V5-Rad6 in a volume of 105 µL. Buffer conditions were 8% glycerol, 7.2 mM Tris-Cl pH 8.0, 26 mM NaCl, and 0.33 mM β-mercaptoethanol. After 10 min incubation at 30 °C, the reaction volume was equally divided into 10 wells of a 96-well plate (Life Technologies #4346907) and covered with an optically clear adhesive seal (Thermo Fisher Scientific #AB1170). The UV lamp was rested directly onto the plate and cross-linking was performed at 4 °C for 30 min at 365 nm. The full reaction was then repooled, boiled in SDS loading buffer, and run on a 12% SDS-polyacrylamide gel (Bio-Rad) followed by Coomassie staining. Gel slices were excised and processed for LC-MS/MS. MS methods have been previously described (69).

RNA-seq and Data Analysis. *S. cerevisiae* and *K. lactis* (KL01) cells were grown in yeast extract-peptone-dextrose media (YPD), harvested at log phase (OD_{600} = 0.8–1.0; measured on an Eppendorf BioPhotometer) and mixed in a 9:1 ratio, respectively, according to the OD_{600} units. Total RNA was extracted from the

spiked-in cell mixture using hot acid phenol (70). The quality of extracted RNA was assessed by gel electrophoresis on 1% TBE gels, and concentrations were determined by Qubit RNA HS kit (Invitrogen). DNase treatment of the RNA samples was done on-column using the RNase-Free DNase Set (QIAGEN) followed by rRNA-depletion using *S. cerevisiae* riboPOOLs probes (siTOOLs Biotech). Sequencing libraries were prepared using the NEBNext® Ultra™ II Directional RNA Library Prep Kit for Illumina (NEB #E7760) coupled with AMPure XP bead purification (Beckman Coulter) with 18 to 22 ng rRNA-depleted RNA as an input. Library quality and fragment distribution were assessed on an Agilent fragment analyzer. Samples were sequenced at the Health Sciences Sequencing Core at the University of Pittsburgh Medical Center (UPMC) Children's Hospital on a NextSeq 500 with 2 × 43-bp paired-end reads. Using STAR (v2.7.5a) aligner (71), all reads were first aligned to the *K. lactis* genome (Ensembl ASM251v1). Reads unmapped to *K. lactis* were designated for alignment to the *S. cerevisiae* S288C genome (Ensembl R64-1-1). Transcript counts were extracted from the BAM files using featureCounts (72). To perform the spike-in correction of *S. cerevisiae* counts, *K. lactis* read counts (mapping to sense strands only) were fed into DESeq2 (54) to estimate replicate-specific size factors. Estimated size factors were then applied to *S. cerevisiae* counts that correspond to protein-coding genes only. Genes with zero counts in all samples were filtered out before the differential expression analysis. To increase the sensitivity of detecting genotype-dependent significant differences, batch effects were mitigated by applying a multifactor design in DESeq2 that includes the genotype and the batch of each sample (i.e., biological replicate number) consistent with how samples were processed in groups of the same biological replicate. PCA plots were derived from counts that underwent variance stabilizing transformation (54). Tidyverse, Psych, ComplexHeatmap, and eulerr R packages were used to produce the correlation plots, heatmap, and Venn diagrams.

Data, Materials, and Software Availability. Genomic data have been deposited in the Gene Expression Omnibus database under accession number GSE218023 (73). All other data are included in the manuscript and/or *SI Appendix*.

ACKNOWLEDGMENTS. We are grateful for the lasting impact of the late Ivan Belashov, who contributed to the early stages of this project during his research rotation in the Arndt lab. We thank Jaehoon Kim for purified recombinant hE1 and yBre1 and to Song Tan for *X. laevis* mononucleosomes. We thank Sarah Hainer, Craig Kaplan, Miler Lee, Andrew VanDemark, Andrea Berman, Laty Cahoon, members of their groups, and all members of the Arndt lab, especially Alex Francette, for many helpful suggestions. We are grateful to Fred Winston for critical reading of the manuscript. This project used the University of Pittsburgh Health Sciences Sequencing Core at UPMC Children's Hospital of Pittsburgh for genomic sequencing experiments and was supported in part by the University of Pittsburgh Center for Research Computing through the resources provided. The mass spectrometry work was supported, in part, by the Indiana Clinical and Translational Science Institute, funded in part by Award Number UL1TR002529 from the NIH, National Center for Advancing Translational Sciences, Clinical and Translational Sciences Award. The research conducted in the Arndt lab was supported by the NIH (R01GM52593 and R35GM141964 to K.M.A.).

Author affiliations: [a]Department of Biological Sciences, University of Pittsburgh, Pittsburgh, PA 15260; and [b]Department of Biochemistry and Molecular Biology, Indiana University School of Medicine, Indianapolis, IN 46202

Author contributions: T.F., B.M.M., and K.M.A. designed research; T.F., B.M.M., N.L.H., D.N.S., and J.D.T. performed research; T.F. and B.M.M. contributed new reagents/analytic tools; T.F., B.M.M., J.D.T., A.L.M., and K.M.A. analyzed data; and T.F., B.M.M., J.D.T., and K.M.A. wrote the paper.

The authors declare no competing interest.

1. J. Chan, A. Kumar, H. Kono, RNAPII driven post-translational modifications of nucleosomal histones. *Trends Genet.* **38**, 1076–1095 (2022).
2. G. Fuchs, D. Hollander, Y. Voichek, G. Ast, M. Oren, Cotranscriptional histone H2B monoubiquitylation is tightly coupled with RNA polymerase II elongation rate. *Genome Res.* **24**, 1572–1583 (2014).
3. J. M. Schulze *et al.*, Splitting the task: Ubp8 and Ubp10 deubiquitinate different cellular pools of H2BK123. *Genes Dev.* **25**, 2242–2247 (2011).
4. A. Wyce *et al.*, H2B ubiquitylation acts as a barrier to Ctk1 nucleosomal recruitment prior to removal by Ubp8 within a SAGA-related complex. *Mol. Cell* **27**, 275–288 (2007).
5. A. B. Fleming, C. F. Kao, C. Hillyer, M. Pikaart, M. A. Osley, H2B ubiquitylation plays a role in nucleosome dynamics during transcription elongation. *Mol. Cell* **31**, 57–66 (2008).
6. K. Batta *et al.*, Genome-wide function of H2B ubiquitylation in promoter and genic regions. *Genes Dev.* **25**, 2254–2265 (2011).
7. Z. Chen *et al.*, High-resolution and high-accuracy topographic and transcriptional maps of the nucleosome barrier. *Elife* **8**, 1–38 (2019).
8. M. Murawska *et al.*, The chaperone FACT and histone H2B ubiquitination maintain *S. pombe* genome architecture through genic and subtelomeric functions. *Mol. Cell* **77**, 501–513.e7 (2020).
9. Z.-W. Sun, C. D. Allis, Ubiquitination of histone H2B regulates H3 methylation and gene silencing in yeast. *Nature* **418**, 104–8 (2002).
10. S. D. Briggs *et al.*, Trans-histone regulatory pathway in chromatin. *Nature* **418**, 498–498 (2002).
11. E. J. Worden, C. Wolberger, Activation and regulation of H2B-Ubiquitindependent histone methyltransferases. *Curr. Opin. Struct. Biol.* **59**, 98–106 (2019).
12. A. Janna, H. Davarinejad, M. Joshi, J. F. Couture, Structural paradigms in the recognition of the nucleosome core particle by histone lysine methyltransferases. *Front. Cell Dev. Biol.* **8**, 1–12 (2020).
13. J. Dover *et al.*, Methylation of histone H3 by COMPASS requires ubiquitination of histone H2B by Rad6. *J. Biol. Chem.* **277**, 28368–28371 (2002).
14. D. G. E. Martin, D. E. Grimes, K. Baetz, L. Howe, Methylation of histone H3 mediates the association of the NuA3 histone acetyltransferase with chromatin. *Mol. Cell Biol.* **26**, 3018–3028 (2006).
15. T. Kim, S. Buratowski, Dimethylation of H3K4 by Set1 recruits the Set3 histone deacetylase complex to 5′ transcribed regions. *Cell* **137**, 259–272 (2009).
16. T. Kim, Z. Xu, S. Clauder-Münster, L. M. Steinmetz, S. Buratowski, Set3 HDAC mediates effects of overlapping noncoding transcription on gene induction kinetics. *Cell* **150**, 1158–1169 (2012).
17. L. Wang, C. Cao, F. Wang, J. Zhao, W. Li, H2B ubiquitination: Conserved molecular mechanism, diverse physiologic functions of the E3 ligase during meiosis. *Nucleus* **8**, 461–468 (2017).
18. K. Robzyk, J. Recht, M. A. Osley, Rad6-Dependent Ubiquitination of Histone H2B in Yeast. *Science* **287**, 501–504 (2000).
19. A. Wood *et al.*, Bre1, an E3 ubiquitin ligase required for recruitment and substrate selection of Rad6 at a promoter. *Mol. Cell* **11**, 267–274 (2003).
20. L. D. Gallego *et al.*, Phase separation directs ubiquitination of gene-body nucleosomes. *Nature* **579**, 592–597 (2020).
21. J. Kim *et al.*, *RAD6*-mediated transcription-coupled H2B ubiquitylation directly stimulates H3K4 methylation in human cells. *Cell* **137**, 459–471 (2009).
22. H. Huang, A. Kahana, D. E. Gottschling, L. Prakash, S. W. Liebman, The ubiquitin-conjugating enzyme Rad6 (Ubc2) is required for silencing in *Saccharomyces cerevisiae*. *Mol. Cell Biol.* **17**, 6693–6699 (1997).
23. C. Hoege, B. Pfander, G.-L. Moldovan, G. Pyrowolakis, S. Jentsch, *RAD6*-dependent DNA repair is linked to modification of PCNA by ubiquitin and SUMO. *Nature* **419**, 135–141 (2002).
24. R. J. Dohmen, K. Madura, B. Bartel, A. Varshavsky, The N-end rule is mediated by the *UBC2(RAD6)* ubiquitin-conjugating enzyme. *Proc. Natl. Acad. Sci. U.S.A.* **88**, 7351–7355 (1991).
25. P. Sung, E. Berleth, C. Pickart, S. Prakash, L. Prakash, Yeast *RAD6* encoded ubiquitin conjugating enzyme mediates protein degradation dependent on the N-end-recognizing E3 enzyme. *EMBO J.* **10**, 2187–2193 (1991).
26. G. M. Silva, D. Finley, C. Vogel, K63 polyubiquitination is a new modulator of the oxidative stress response. *Nat. Struct. Mol. Biol.* **22**, 116–123 (2015).
27. V. Simões *et al.*, Redox-sensitive E2 Rad6 controls cellular response to oxidative stress via K63-linked ubiquitination of ribosomes. *Cell Rep.* **39**, 110860 (2022).
28. S. W. Liebman, G. Newnam, A ubiquitin-conjugating enzyme, *RAD6*, affects the distribution of Ty1 retrotransposon integration positions. *Genetics* **133**, 499–508 (1993).
29. S. Picologlou, N. Brown, S. W. Liebman, Mutations in *RAD6*, a yeast gene encoding a ubiquitin-conjugating enzyme, stimulate retrotransposition. *Mol. Cell Biol.* **10**, 1017–1022 (1990).
30. A. M. Francette, S. A. Tripplehorn, K. M. Arndt, The Paf1 complex: A keystone of nuclear regulation operating at the interface of transcription and chromatin. *J. Mol. Biol.* **433**, 166979 (2021).
31. A. Wood, J. Schneider, J. Dover, M. Johnston, A. Shilatifard, The Paf1 complex is essential for histone monoubiquitination by the Rad6-Bre1 complex, which signals for histone methylation by COMPASS and Dot1p. *J. Biol. Chem.* **278**, 34739–34742 (2003).
32. J. Kim, R. G. Roeder, Direct Bre1-Paf1 complex interactions and RING Fingerindependent Bre1-Rad6 interactions mediate histone H2B ubiquitylation in yeast. *J. Biol. Chem.* **284**, 20582–20592 (2009).
33. A. S. Piro, M. K. Mayekar, M. H. Warner, C. P. Davis, K. M. Arndt, Small region of Rtf1 protein can substitute for complete Paf1 complex in facilitating global histone H2B ubiquitylation in yeast. *Proc. Natl. Acad. Sci. U.S.A.* **109**, 10837–10842 (2012).
34. S. B. Van Oss *et al.*, The histone modification domain of Paf1 complex subunit Rtf1 directly stimulates H2B ubiquitylation through an interaction with Rad6. *Mol. Cell* **64**, 815–825 (2016).
35. M. H. Warner, K. L. Roinick, K. M. Arndt, Rtf1 is a multifunctional component of the Paf1 complex that regulates gene expression by directing cotranscriptional histone modification. *Mol. Cell Biol.* **27**, 6103–6115 (2007).
36. Q.-F. Cao *et al.*, Characterization of the human transcription elongation factor Rtf1: Evidence for nonoverlapping functions of Rtf1 and the Paf1 complex. *Mol. Cell Biol.* **35**, 3459–3470 (2015).
37. B. N. Tomson, C. P. Davis, M. H. Warner, K. M. Arndt, Identification of a role for histone H2B ubiquitylation in noncoding RNA 3′-end formation through mutational analysis of Rtf1 in *Saccharomyces cerevisiae*. *Genetics* **188**, 273–289 (2011).
38. F. Chen *et al.*, Biochemical insights into Paf1 complex-induced stimulation of Rad6/Bre1-mediated H2B monoubiquitination. *Proc. Natl. Acad. Sci. U.S.A.* **118**, 1–11 (2021).
39. D. Finley, H. D. Ulrich, T. Sommer, P. Kaiser, The Ubiquitin-Proteasome System of *Saccharomyces cerevisiae*. *Genetics* **192**, 319–360 (2012).
40. J. W. Chin, A. B. Martin, D. S. King, L. Wang, P. G. Schultz, Addition of a photocrosslinking amino acid to the genetic code of *Escherichia coli*. *Proc. Natl. Acad. Sci. U.S.A.* **99**, 11020–11024 (2002).
41. A. Wittelsberger, D. F. Mierke, M. Rosenblatt, Mapping ligand-receptor interfaces: Approaching the resolution limit of benzophenone-based photoaffinity scanning. *Chem. Biol. Drug Des.* **71**, 380–383 (2008).
42. F. Chen *et al.*, Crystal structure of the core module of the yeast Paf1 complex. *J. Mol. Biol.* **434**, 167369 (2022).
43. A. D. Wier, M. K. Mayekar, A. Héroux, K. M. Arndt, A. P. VanDemark, Structural basis for Spt5-mediated recruitment of the Paf1 complex to chromatin. *Proc. Natl. Acad. Sci. U.S.A.* **110**, 17290–17295 (2013).

44. D. K. Worthylake, S. Prakash, L. Prakash, C. P. Hill, Crystal structure of the *Saccharomyces cerevisiae* ubiquitin-conjugating enzyme Rad6 at 2.6 Å resolution. *J. Biol. Chem.*, **273**, 6271–6276 (1998).
45. A. M. Waterhouse, J. B. Procter, D. M. A. Martin, M. Clamp, G. J. Barton, Jalview version 2-a multiple sequence alignment editor and analysis workbench. *Bioinformatics* **25**, 1189–1191 (2009).
46. A. Bachmair, D. Finley, A. Varshavsky, *In vivo* half-life of a protein is a function of its amino-terminal residue. *Science* **234**, 179–186 (1986).
47. B. Bartel, I. Wünning, A. Varshavsky, The recognition component of the N-end rule pathway. *EMBO J.* **9**, 3179–3189 (1990).
48. W. W. Hwang *et al.*, A conserved RING finger protein required for histone H2B monoubiquitination and cell size control. *Mol. Cell* **11**, 261–266 (2003).
49. R. Evans *et al.*, Protein complex prediction with AlphaFold-Multimer. *bioRxiv [Preprint]* (2021). https://doi.org/10.1101/2021.10.04.463034 (Accessed 10 March 2022).
50. J. Jumper *et al.*, Highly accurate protein structure prediction with AlphaFold. *Nature* **596**, 583–589 (2021).
51. J. W. Chin *et al.*, An expanded eukaryotic genetic code. *Science* **301**, 964–967 (2003).
52. R. Meas, P. Mao, Histone ubiquitylation and its roles in transcription and DNA damage response. *DNA Repair (Amst).* **36**, 36–42 (2015).
53. J. F. Watkins, P. Sung, S. Prakash, L. Prakash, The extremely conserved amino terminus of *RAD6* ubiquitin-conjugating enzyme is essential for amino-end rule-dependent protein degradation. *Genes Dev.* **7**, 250–261 (1993).
54. M. I. Love, W. Huber, S. Anders, Moderated estimation of fold change and dispersion for RNA-seq data with DESeq2. *Genome Biol.* **15**, 550 (2014).
55. V. Pagé *et al.*, Histone H2B ubiquitylation regulates histone gene expression by suppressing antisense transcription in fission yeast. *Genetics* **213**, 161–172 (2019).
56. G. Freiberg, A. D. Mesecar, H. Huang, J. Y. Hong, S. W. Liebman, Characterization of novel *rad6/ubc2* ubiquitin-conjugating enzyme mutants in yeast. *Curr. Genet.* **37**, 221–233 (2000).
57. M. Pan *et al.*, Structural insights into Ubr1-mediated N-degron polyubiquitination. *Nature* **600**, 334–338 (2021).
58. Z. Tokgöz *et al.*, E1–E2 interactions in ubiquitin and Nedd8 ligation pathways. *J. Biol. Chem.* **287**, 311–321 (2012).
59. P. J. Winn, T. L. Religa, J. N. D. Battey, A. Banerjee, R. C. Wade, Determinants of functionality in the ubiquitin conjugating enzyme family. *Structure* **12**, 1563–1574 (2004).
60. R. Gatta *et al.*, An acetylation-monoubiquitination switch on Lysine 120 of H2B. *Epigenetics* **6**, 630–637 (2011).
61. M. Crespo *et al.*, Systematic genetic and proteomic screens during gametogenesis identify H2BK34 methylation as an evolutionary conserved meiotic mark. *Epigenet. Chromatin* **13**, 35 (2020).
62. E. Turco, L. D. Gallego, M. Schneider, A. Köhler, Monoubiquitination of histone H2B is intrinsic to the Bre1 RING domain-Rad6 interaction and augmented by a second Rad6-binding site on Bre1. *J. Biol. Chem.* **290**, 5298–5310 (2015).
63. L. D. Gallego *et al.*, Structural mechanism for the recognition and ubiquitination of a single nucleosome residue by Rad6-Bre1. *Proc. Natl. Acad. Sci. U.S.A.* **113**, 10553–10558 (2016).
64. P. K. Shukla *et al.*, Structure and functional determinants of Rad6–Bre1 subunits in the histone H2B ubiquitin-conjugating complex. *Nucleic Acids Res.* **51**, 2117–2136 (2023).
65. M. Shi *et al.*, Structural basis for the Rad6 activation by the Bre1 N-terminal domain. *Elife* **12**, e84157 (2023).
66. C. E. Cucinotta, A. E. Hildreth, B. M. McShane, M. K. Shirra, K. M. Arndt, The nucleosome acidic patch directly interacts with subunits of the Paf1 and FACT complexes and controls chromatin architecture *in vivo*. *Nucleic Acids Res.* **47**, 8410–8423 (2019).
67. F. Winston, C. Dollard, S. L. Ricupero-Hovasse, Construction of a set of convenient *Saccharomyces cerevisiae* strains that are isogenic to S288C. *Yeast* **11**, 53–55 (1995).
68. V. V. Kushnirov, Rapid and reliable protein extraction from yeast. *Yeast* **16**, 857–860 (2000).
69. R. Dronamraju *et al.*, Casein kinase II phosphorylation of Spt6 enforces transcriptional fidelity by maintaining Spn1-Spt6 interaction. *Cell Rep.* **25**, 3476–3489.e5 (2018).
70. M. A. Collart, S. Oliviero, Preparation of yeast RNA. *Curr. Protoc. Mol. Biol.* **23**, 13.12.1–13.12.5 (1993).
71. A. Dobin *et al.*, STAR: Ultrafast universal RNA-seq aligner. *Bioinformatics* **29**, 15–21 (2013).
72. Y. Liao, G. K. Smyth, W. Shi, FeatureCounts: An efficient general purpose program for assigning sequence reads to genomic features. *Bioinformatics* **30**, 923–930 (2014).
73. T. Fetian *et al.*, Paf1 complex subunit Rtf1 stimulates H2B ubiquitylation by interacting with the highly conserved N-terminal helix of Rad6. *Gene Expression Omnibus*. https://www.ncbi.nlm.nih.gov/geo/query/acc.cgi?acc=GSE218023 (Accessed 15 November 2022).